JOURNAL OF GEOPHYSICAL RESEARCH VOLUME 67, NO. 5 MAY 1962

Source-Mechanism from Spectra of Long-Period Seismic Surface-Waves

1. The Mongolian Earthquake of December 4, 1957[1]

ARI BEN-MENAHEM AND M. NAFI TOKSÖZ

Seismological Laboratory
California Institute of Technology, Pasadena

Abstract. The Pasadena seismograms of the Mongolian earthquake of December 4, 1957, were studied. Mantle Rayleigh waves R_3, R_4, R_5, and R_6 were separated, digitized, filtered, and Fourier-analyzed. After the evaluation of the phase velocities and the absorption coefficients from amplitude ratios R_3/R_5 and R_4/R_6 the directivity was computed from the amplitude ratio of R_3/R_4. A fault of 560 km, with an azimuth of 100°, and a rupture velocity of 3.5 km/sec gave the best fit to the observed directivity. Auxiliary data from aftershock distribution, initial motions, air waves from the main shock, and geological surveys of the fault area seem to support these findings. The phase spectra of R_3 and R_4 were corrected for the propagation phase and the instrumental phase shift to obtain the initial phases at the source. A rough estimate of the depth of faulting is obtained on the basis of the calculated strain release and observed displacements at the fault.

INTRODUCTION

On December 4, 1957, at about 03 37 45, a destructive earthquake of magnitude 7¾ to 8, known as the Mongolian or the Gobi-Altai earthquake, occurred in the Gurban-Bogdo Mountains in the southern part of Outer Mongolia. The epicenter was located at 45.25°N, 99.4°E. Studies of the epicentral region [*Florensov*, 1958] established that the shock caused great destruction, creating numerous fractures, cavings, and landslides. The main fracture could be traced uninterruptedly for 270 km. The earthquake displaced the Yihe-Bodgo massif (which is about 100 km long and 3800 m high) 3 to 3.5 m toward the east and lifted it 2 to 6 m. Sensitive microbarographs recorded air waves at a distance of 2440 km from the epicenter. About 200 large aftershocks, in an area 500 km long and 200 km wide, were reported by the Soviet station-network during the first year following the main shock. Weak body waves with unclear arrivals and high-intensity surface waves were recorded by most of the seismological stations around the world, indicating a shallow focus with large dimensions. At Pasadena, for example, the Airy phase of R_3 which traveled about 150,000 km from the source could still be seen in spite of the unfavorable azimuth of the station with respect to the fault (Fig. 1) and the effective high-pass filtering of the 30–90 seismograph system [*Press, Ewing, and Lehner*, 1958; *Gilman*, 1960]. With the purpose of determining the fault length, the rupture velocity, if any, and other derivable parameters of the source, we undertook the study of this earthquake. The only useful records available in Pasadena were those of the 30–90 seismograph. The vertical component seismogram showed the largest amplitudes and there was no interference due to G waves. Therefore, it was used in the analysis.

DATA ANALYSIS

The Pasadena seismogram of the Mongolian earthquake of December 4, 1957, is shown in Figure 2. Because of their large amplitudes and light traces it was impossible to follow the R_1 and R_2 trains. However, R_3 through R_6 could be seen quite easily. Dispersion and high-frequency noise made it hard to locate the onsets of the wave trains; we therefore preferred to assign a group-velocity window in order to determine the length and the beginning of each wave train. For the maximum group velocity we chose the value of 4.10 km/sec, which corresponds to a

[1] Contribution 1052, Division of Geological Sciences, California Institute of Technology.

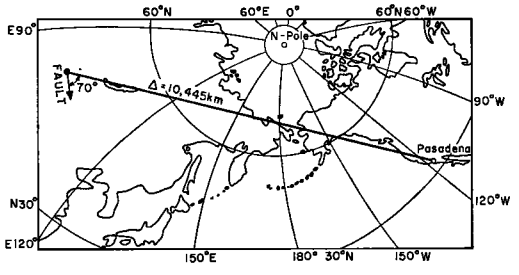

Fig. 1. Position of Pasadena relative to the fault of the Mongolian earthquake of December 4, 1957. Black line indicates part of great circle traveled by R_1.

period of about 360 sec. For the minimum group velocity we chose the value of 3.45 km/sec, which corresponds to the latest group arrival of the Airy phase. The epicentral distance to Pasadena (34°08′54″N, 118°10′18″W) was $\Delta_1 = 10{,}445$ km with the azimuth of 30.45° from the source. Times of the beginnings and ends of the digitized wave trains are given in Table 1. It is hard to check the mutual fit of the chosen onsets but the ends of the trains fell right after their Airy phases. This gave us confidence in the choice of the velocity window. Each wave train was then digitized at 3-sec intervals and Fourier analyzed using the Caltech–Jet Propulsion Laboratory's IBM 7090 electronic computer. Before the Fourier analysis the data were filtered with a 19-coefficient triangular low-pass digital filter. The transfer function and the response of the filter are shown in Figure 3. The separated but unfiltered records are shown in Figure 4 and the results after filtering are shown in Figure 5. Before and after the filtering either the mean or the linear trend was removed from the data. To check on the numerical integration involved in Fourier analysis, the data were analyzed using both modified trapezoidal rule and Filon's method [*Tranter*, 1956] and no appreciable difference was found between the results. A frequency interval of 0.5×10^{-4} cps was chosen for the analysis. The separated unfiltered wave forms, as compared with the filtered ones, are given in Figures 4 and 5. The amplitude spectra of the filtered R_3 and R_4 are shown in Figures 6 and 7. From the amplitude and the phase spectra we determined the following entities:

Absorption coefficients. The attenuation function $\gamma(\omega)$ is defined by

$$A_n(\omega)/A_{n+2}(\omega) = \exp\,[40{,}030\,\gamma(\omega)] \qquad (1)$$

where $A_n(\omega)$ is the amplitude spectrum of a surface wave of order n. The spectra of R_3, R_4, R_5, R_6 have been smoothed and $\gamma(\omega)$ was computed independently from R_3/R_5 and from R_4/R_6, to check whether there is any effect due to the asymmetry of the source. Another check was made by a direct measurement of the absorption coefficient from the record at the Airy phase using the formula

$$\ln A_n/A_{n+2}|_{T=T_0} = 40{,}030\gamma_0 + \tfrac{1}{3}\ln \Delta_{n+2}/\Delta_n \qquad (2)$$

Results are exhibited in Figure 8. The curve has a knee at $f = 0.0075$ sec^{-1}, and from there on it decreases slightly to an asymptotic value at high frequencies. Comparison with values obtained for the Chilean earthquake of May 22, 1960 [*Press, Ben-Menahem, and Toksöz*, 1961], indicates a fair fit for periods longer than 140

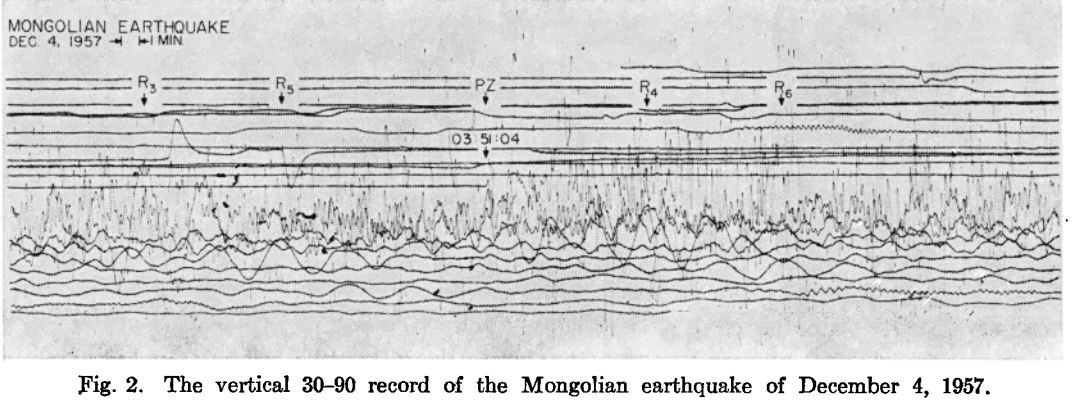

Fig. 2. The vertical 30–90 record of the Mongolian earthquake of December 4, 1957.

Table 1. The Digitized Phases (eP = 03 51 04)

Phase	Distance Traveled, km	Onset of Wave, h m s	End of Wave, h m s	Length of Record, sec	Digitized Points
R_3	50,475	07 03 33	07 39 33	2160	721
R_4	69,615	08 20 33	09 12 33	3120	1041
R_5	90,505	09 45 33	10 54 33	4140	1381
R_6	109,645	11 02 33	12 26 33	5040	1681

sec. For shorter periods the Mongolian earthquake shows a consistent lower attenuation.

Phase velocities. The phase velocities were determined separately from $R_5 - R_3$ and $R_6 - R_4$ by means of the formula

$$C(T) = \frac{40{,}030}{\partial t + T(\partial\varphi + N - \frac{1}{2})} \qquad (3)$$

where ∂t is the time interval between the beginnings of the windows, $\partial\varphi(T)$ is the spectral phase difference for R_5 and R_3 (i.e. $R_5 - R_3$) or R_6 and R_4, N = a constant integer, and $-\frac{1}{2}$ corresponds to the phase shift due to two extra polar passages of R_5 or R_6 [*Brune, Nafe, and Alsop,* 1961]. We found that the phases were ill-behaved near the zeros of the corresponding amplitude spectra and also at short periods. This limited the range of dependability from 340 sec to 130 sec. Within this range, however, the values determined from $R_5 - R_3$ and $R_6 - R_4$ agree very closely, the discrepancy being less than ½ per cent. The values obtained are also in agreement with the results of other investigators [*Brune, Benioff, and Ewing,* 1961; *Brune,* 1961; *Brune, Nafe, and Alsop,* 1961]. Results are given in Table 2 and Figure 9.

Directivity. Ben-Menahem [1961] has investigated the effect of the source finiteness on radiation of seismic waves from finite sources. Solving the wave equation for a steady-state point source yields the surface displacements in an integral representation, from which the surface wave contribution is easily separated. To obtain the radiation pattern due to a horizontally moving source, the point-source displacements are integrated over the entire fault. The final results contain the finiteness effect of the source as a factor of the form $(\sin x/x)e^{-ix}$ where $x = (\pi fb/C)\ (C/V - \cos\theta_0)$, b being the fault length, f the frequency, C the phase velocity, V the velocity of rupture, and θ_0 the angle between the fault line and the great circle from the fault to the recording station. To be able to derive the source parameters from the displacements we must eliminate the effect of the medium and the source's time function on the displacements. This is achieved by defining the directivity function which is equal to the ratio of spectral amplitudes of waves leaving the source in opposite directions. The convention is followed that the numerator of the ratio corresponds to waves leaving the source in the direction of rupture. The directivity is given by

$$D = \frac{\left|\left(\frac{C}{V} + \cos\theta_0\right)\left[\sin\frac{\pi bf}{C}\left(\frac{C}{V} - \cos\theta_0\right)\right]\right|}{\left|\left(\frac{C}{V} - \cos\theta_0\right)\left[\sin\frac{\pi bf}{C}\left(\frac{C}{V} + \cos\theta_0\right)\right]\right|} \qquad (4)$$

The experimental directivity was obtained from R_3 and R_4 by dividing the amplitudes of $R_3(\omega)$ pointwise with those of $R_4(\omega)$ corrected for absorption. The theoretical curve is calculated from (4) by assuming a unilateral horizontal fault movement with a constant velocity of rupture V and constant strength. A theoretical curve was then fitted to the experimental data. This was done by choosing first a rough value

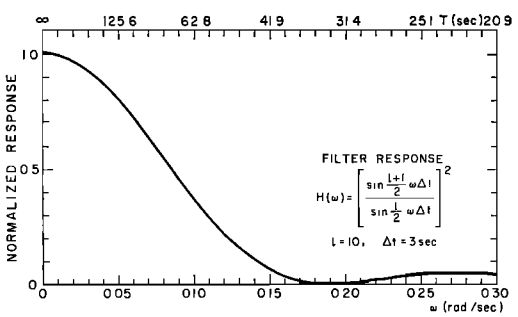

Fig. 3. Response of the triangular filter used to eliminate high-frequency noise from mantle Rayleigh waves R_3 and R_4.

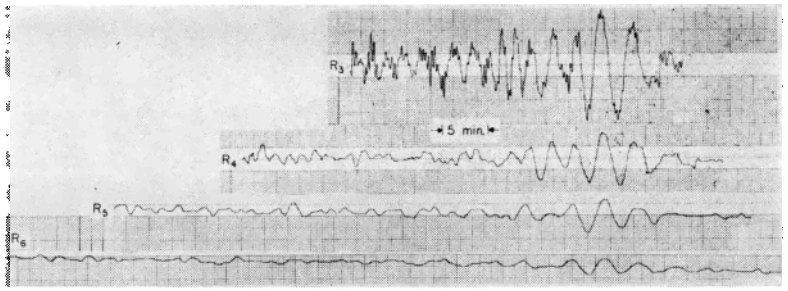

Fig. 4. The unfiltered mantle Rayleigh waves R_3, R_4, R_5, R_6 of the Mongolian earthquake of December 4, 1957.

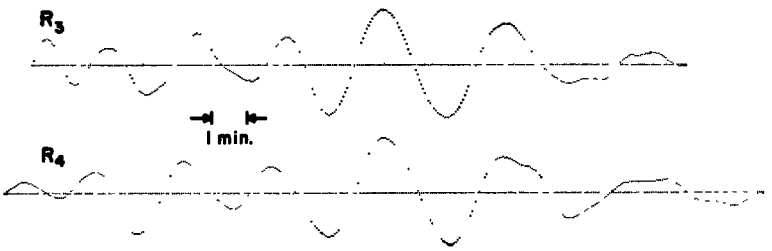

Fig. 5. Portion of the filtered mantle Rayleigh waves R_3 and R_4.

for θ_0 and b from the known fault trace (Fig. 10) and then improving the match for b, V, and θ_0 by the trial and error method. The best match was obtained with $b = 560$ km, $V = 3.5$ km/sec, and azimuth of 100° ($\theta_0 = 70°$). These results are not necessarily unique, but the existence of a different reasonable set is highly improbable if not altogether impossible. A close examination of the results (Fig. 11) raises some questions which need clarification. In the first place we notice that the experimental directivity contains a high-frequency oscillation. The origin of these oscillations goes back to the individual spectra of R_3 and R_4 and will be dealt with in the section on error analysis. A more serious point is the absence of the first maximum in the observed directivity. This occurs around a period of 200 sec. A coherence test disclosed that the data in this frequency band were most dependable (see also phase velocities in Table 2). To check for a possible narrow infinity we swept the band in question with a finer spacing, but to no effect. Modification of the theoretical model was tried: for a source with variable strength, $L = L_0 e^{-2\xi/b_0}$, and $0 \leq \xi \leq b$, the directivity becomes

$$D = \frac{\left\{\sin^2 X_1 + \sinh^2\left(\frac{b}{b_0}\right)\right\}^{1/2}}{\left\{\sin X_2^2 + \sinh^2\left(\frac{b}{b_0}\right)\right\}^{1/2}} \frac{\left\{X_2^2 + \left(\frac{b}{b_0}\right)^2\right\}^{1/2}}{\left\{X_1^2 + \left(\frac{b}{b_0}\right)^2\right\}^{1/2}} \tag{5}$$

where

$$X_1 = \frac{\pi f b}{C}\left(\frac{C}{V} - \cos\theta_0\right)$$

and

$$X_2 = \frac{\pi f b}{C}\left(\frac{C}{V} + \cos\theta_0\right)$$

If we require that $L(b) = (1/\beta)L_0$ then $b/b_0 = \frac{1}{2}\log_e\beta$. Thus β is a parameter which governs the rate of decay of the source along the fault. The directivity was programed for various values of β. It was found that the effect of a decaying source was to flatten *all* the extremes of the directivity. An example with $\beta = e$ is shown in Figure 11. The idea of bidirectional faulting was also tried. Assuming that the strength of either part can be taken propor-

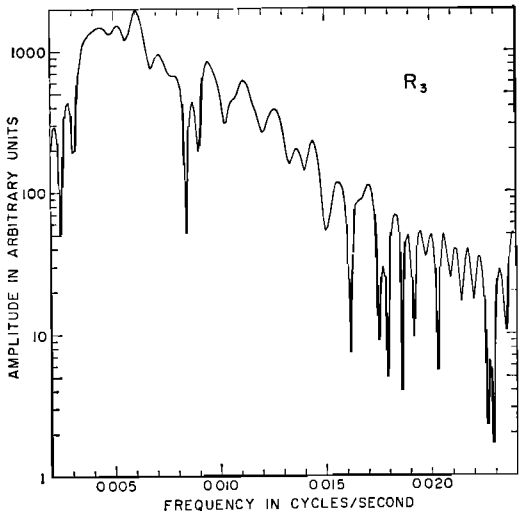

Fig. 6. Amplitude spectrum of R_3.

tional to its length, we obtain for the directivity

$$D = \left\{ \frac{A_1^2 + \left(\frac{b_2}{b_1}\right)^2 B_1^2 - 2\frac{b_2}{b_1} A_1 B_1 \cos\phi}{A_2^2 + \left(\frac{b_2}{b_1}\right)^2 B_2^2 - 2\frac{b_2}{b_1} A_2 B_2 \cos\phi} \right\}^{1/2} \tag{6}$$

where

$$A_1 = \frac{\sin\left[\frac{\pi f b_1}{C}\left(\frac{C}{V} - \cos\theta_0\right)\right]}{\frac{\pi f b_1}{C}\left(\frac{C}{V} - \cos\theta_0\right)}$$

$$B_1 = \frac{\sin\left[\frac{\pi f b_2}{C}\left(\frac{C}{V} + \cos\theta_0\right)\right]}{\frac{\pi f b_2}{C}\left(\frac{C}{V} + \cos\theta_0\right)}$$

$$A_2 = \frac{\sin\left[\frac{\pi f b_1}{C}\left(\frac{C}{V} + \cos\theta_0\right)\right]}{\frac{\pi f b_1}{C}\left(\frac{C}{V} + \cos\theta_0\right)} \tag{7}$$

$$B_2 = \frac{\sin\left[\frac{\pi f b_2}{C}\left(\frac{C}{V} - \cos\theta_0\right)\right]}{\frac{\pi f b_2}{C}\left(\frac{C}{V} - \cos\theta_0\right)}$$

$$\phi = \pi f\left(\frac{b_1 - b_2}{V} - \frac{b_1 + b_2}{C}\cos\theta_0\right)$$

To ease the programing the phase velocity was expressed by the function

$$C(T) = 3.80 + 4.70\frac{T}{1000} - 0.25 \cdot \sin\left(\frac{T}{100} + 0.28\right) \quad 50 < T < 600 \tag{8}$$

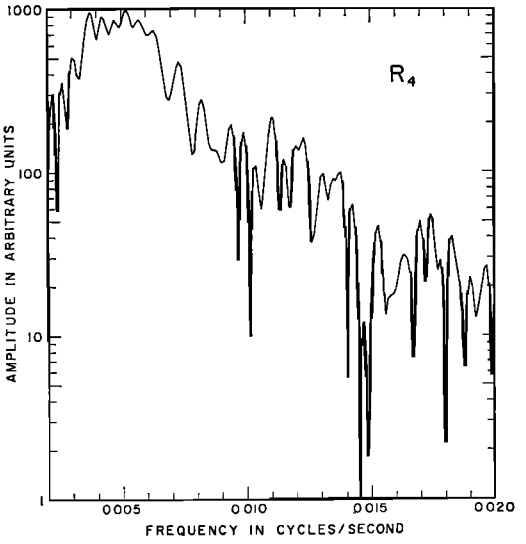

Fig. 7. Amplitude spectrum of R_4.

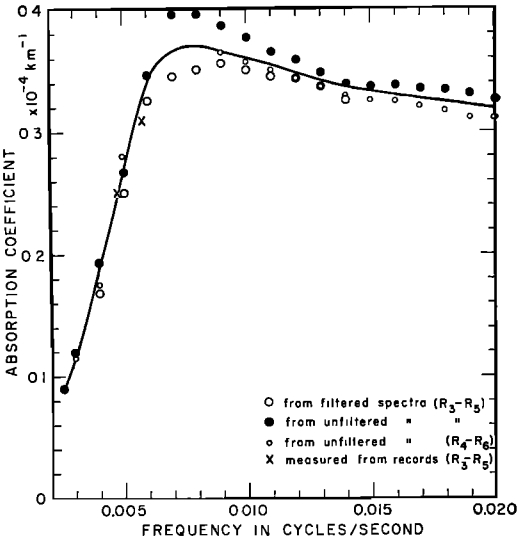

Fig. 8. Attenuation curve as obtained from the amplitude spectra of $R_3 - R_5$, $R_4 - R_6$. The attenuation at the Airy phase and at $T = 170$ sec were also evaluated directly from the records.

TABLE 2. Observed Phase Velocities for Mantle Rayleigh Waves
$N = -7$ $t = 9270$ sec

Frequency, cps	Period, sec	Phase Velocities, km/sec			
		From $R_5 - R_3$,	From $R_6 - R_4$,	Other Results	Eq. 8
0.0025	400.00			5.985 As (3)	5.907
0.0026	384.61				5.816
0 0027	370 37			5 760 Ch (3)	5.727
0.0028	357.14	5.630			5.641
0 0029	344.83	5.557			5.559
0.0030	333.33	5.488		5.503 As (3)	5.480
0.0031	322.58	5.418	5.434		5.405
0.0032	312.50	5.361	5.349		5.339
0.0033	303.03	5.304	5.307	5.284 Ch (1)	5.266
0.0034	294.12	5.232	5.247		5.202
0.0035	285.71	5.175	5.173	5.183 As (3)	5.142
0.0036	277.78	5.121	5.102	5.101 Ch (1)	5.084
0.0037	270.27	5.063	5.058		5.031
0.0038	263.16	5.006	5.015		4.980
0.0039	256.41	4.960	4.959		4.932
0.0040	250.00	4.916	4.921	4.940 As (3)	4.886
0.0041	243.90	4.865	4.876	4.840 Ch (1)	4.843
0.0042	238.09	4.820	4.825		4.803
0.0043	232.56	4.784	4.789		4.765
0.0044	227.27	4.747	4.736	4.737 Al (2)	4.730
0.0045	222.22	4.713	4.708	4.717 As (3)	4.696
0.0046	217.39	4.685	4.690	4.682 Al (2)	4.663
0.0047	212.77	4.654	4.644	4.647 Al (2)	4.632
0.0048	208.33	4.615	4.622		4.604
0.0049	204.08	4.591	4.603		4.576
0.0050	200.00	4.570	4.571	4.568 As (3)	4.550
0.0051	196.08	4.541	4.552		4.525
0.0052	192.31	4.515	4.520	4.509 Al (2)	4 502
0.0053	188.68	4.498	4.489		4.480
0.0054	185.19	4.481	4.480		4.459
0.0055	181.82	4.457	4.455	4.459 Al (2)	4.438
0.0056	178.57	4.436	4.443		4.419
0.0057	175.44	4.420	4.435		4.401
0.0058	172.41	4.400	4.421	4.413 Al (2)	4.383
0.0059	169.49	4.384	4.391		4.367
0.0060	166.67	4.372	4.375	4.380 As (3)	4.351
0.0061	163.93	4.361	4.367	4.371 Al (2)	4.335
0.0062	161.29	4.351	4.345	4.357 Al (2)	4.321
0.0063	158.73	4.339	4.340		4.307
0.0064	156.25	4.319		4.334 Al (2)	4.293
0.0065	153.85	4.301			4.281
0.0066	151.52	4.290		4.311 Al (2)	4.268
0.0067	149.25	4.284		4.302 Al (2)	4.256
0.0068	147.06	4.281			4.245
0.0069	144.93	4 277			4.234
0.0070	142.86	4.270		4.246 As (3)	4.224
0.0071	140.84	4.266		4.258 Al (2)	4.213
0.0072	138.89	4.257			4.204
0.0073	136.99	4.253			4.194
0.0074	135.14	4.249			4.185
0.0075	133.33	4.242			4.177
0.0076	131.58	4.236			4.168
0.0077	129.87	4.229		4.217 Al (2)	4.160
0.0078	128.21	4.219			4.152
0.0079	126.58	4.211			4.145
0.0080	125.00	4.205		4.164 As (3)	4.137

TABLE 2. Continued

Frequency, cps	Period, sec	Phase Velocities, km/sec			
		From $R_5 - R_3$,	From $R_6 - R_4$,	Other Results	Eq. 8
0.0081	123.46	4.201			4.131
0.0082	121.95	4.188			4.124
0.0083	120.48	4.177			4.117
0.0084	119.05	4 171			4.111
0.0085	117.65	4.159			4.105
0.0086	116.28	4 158			4.098
0.0087	114.94	4.155			4.093
0.0088	113.64	4.151			4.087
0.0089	112.36	4.144			4.081
0.0090	111.11	4.136		4.102 As (3)	4.076
0.0091	109.89	4.133			4.071
0.0092	108.70	4.130			4.066
0.0093	107.53	4.122			4.061
0.0094	106.38	4.120			4.056
0.0095	105.26	4.116			4.052
0.0096	104.17	4.111			4.047
0.0097	103.09	4.107			4.043
0.0098	102.04	4.101			4.039
0.0099	101.01	4.096			4.035
0.0100	100.00	4.093		4.054 As (3)	4.030

As = Assam earthquake of August 15, 1950.
Al = Alaskan earthquake of July 10, 1958.
Ch = Chilean earthquake of May 22, 1960.

(1) = *Brune, Benioff, and Ewing* [1961].
(2) = *Brune* [1961].
(3) = *Brune, Nafe, and Alsop*, [1961].

Equation 8 is tabulated in Table 2. The differences between the observed data and the values given by (8) are mostly less than 1 per cent. The directivity for case $b_1 = 420$ km, $b_2 = 140$ km, $V = 3.5$ km/sec, and $\theta_0 = 70°$ is shown in Figure 11. It is apparent that the fault of the Mongolian earthquake was not of this type. Several models of bidirectional faultings were tried, none of which fitted the observed directivity. A variable rupture velocity was also considered. Here the directivity is given by

$$D = \left\{\frac{A_-^2 + B_-^2}{A_+^2 + B_+^2}\right\}^{1/2} \tag{9}$$

with

$$V = V_0/g(\xi)$$

$$A_\mp = \int_0^b \cos\left\{\frac{\omega}{C}\xi\left[\frac{C}{V_0}\,g(\xi) \mp \cos\theta_0\right]\right\}d\xi$$

$$B_\mp = \int_0^b \sin\left\{\frac{\omega}{C}\xi\left[\frac{C}{V_0}\,g(\xi) \mp \cos\theta_0\right]\right\}d\xi \tag{10}$$

It is easy to show by means of simple examples that the missing infinity cannot be accounted for by this model. Two alternatives, which are not mutually exclusive, could be raised to explain this phenomenon: (1) nonlinear processes which are responsible for a feedback of power into the Airy phase from neighboring frequencies or (2) a complexity at the source which tended to limit the asymmetrical radiation to higher frequencies only. The partial disagreement between the observed data and the theoretical model, together with the oscillatory ripple present in the observed directivity, may give rise to some doubts as to the dependability of its other extremes. This is definitely ruled out in light of the relative strength of the other zeros and infinities, which deviate from the mean oscillation level by at least a factor of 10. They were present in the data regardless of the method of analysis, filtering, and detrending. It is also highly improbable that random noise will fit the predicted theoretical scheme.

Initial phases. The initial phase of a seismic source is defined as the phase spectrum of its time function (that is, the phase of its Fourier transform). In the case of a finite moving source the initial phase will incorporate an additional

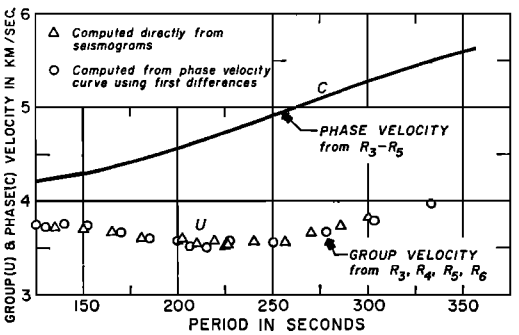

Fig. 9. Phase and group velocities of mantle Rayleigh waves from the Mongolian earthquake of December 4, 1957, recorded at Pasadena, California.

phase due to the finiteness of the source. For example, in the case of a moving strike-slip fault there is a phase shift of $(\pi bf/2C)$ $(C/V - \cos\theta_0)$ radian [*Ben-Menahem*, 1961]. Table 3 includes the initial phases of a few elementary time functions. To recover the initial phase from the spectrum of mantle Rayleigh waves one should correct for the propagation phase, the instrumental phase shift, and the window effect. Thus we have

$$ft_n + \varphi_n(f) + \varphi_{inst} = f\frac{\Delta_n}{C} + \phi_0(f) + (M + \tfrac{1}{2}) \qquad (11)$$

where t_n is the time lag of the beginning of the spectral window with respect to the time of origin, φ_n is the Fourier-analysis phase, Δ_n is the epicentral distance of a surface wave of order n, $\phi_0(f)$ is the sought initial phase, and M is an integer. Phase shifts due to absorption have not been considered. Phases are measured in parts of a circle. The initial phases of R_3 and R_4 were calculated from the corresponding phase spectra and the known phase velocities using the formulas

$$\begin{aligned} -(\phi_0)_3 &= 9.5 - f\left(12{,}348 - \frac{50{,}475}{C}\right) - \varphi_3(f) \\ -(\phi_0)_4 &= 13.25 - f\left(16{,}968 - \frac{69{,}615}{C}\right) - \varphi_4(f) \end{aligned} \qquad (12)$$

A graphical display is given in Figure 12. Some immediate conclusions may be drawn from this figure:

1. The finiteness effect was smaller than that predicted by the theory. As a result the initial phases of R_3 and R_4 fall close to each other. This occurred mostly in the frequency band for which the observed directivity disobeyed the theoretical predictions.

2. The initial phase does not seem to be constant for this earthquake. Results for the Alaskan earthquake of July 10, 1958 [*Brune*, 1961], and the Chilean earthquake of May 22, 1960 [*Brune, Benioff, and Ewing*, 1961], do not agree with our findings. We wish to elaborate somewhat on this important point. The initial phase at the source may be separated into two parts, a phase which is due to the strain-release time function at a point on the fault and the phase retardation due to the finiteness and the motion of the source. A constant initial phase means either that both these contributions are constant or that they cancel each other along the entire frequency spectrum. It is possible to put forward a source model with a constant-phase time function (see Appendix). The finiteness phase, however, can never be constant over the entire spectrum, and for faults of the order of 1000 km it should be easily detectable. Thus a constant initial phase in the case of the Chilean earthquake can mean that the two components of the initial-phase function annihilated each other, at least in the measured period range 215 to 550 sec, reported by *Brune, Benioff, and Ewing* [1961]. The question now arises whether the

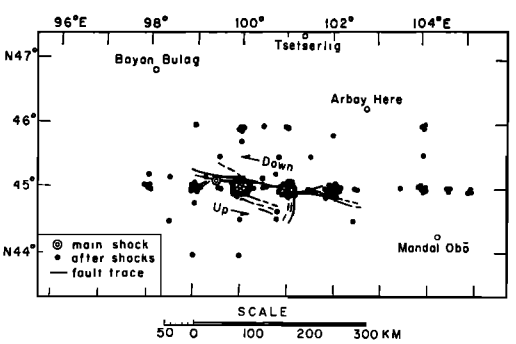

Fig. 10. Map of part of Outer Mongolia showing traces of visible faults and distribution of aftershocks of the Mongolian earthquake of December 4, 1957.

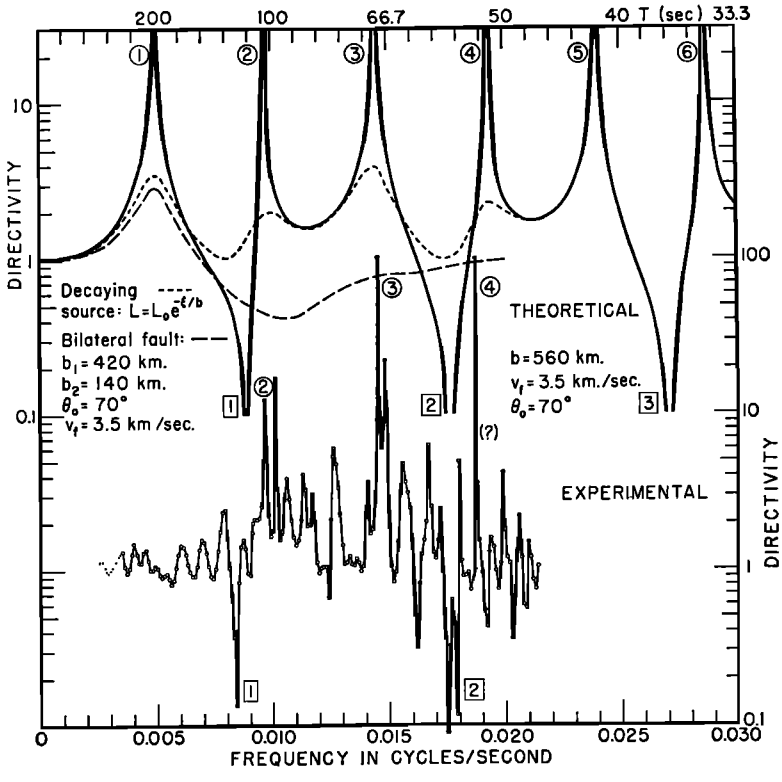

Fig. 11. Theoretical versus experimental directivity for mantle Rayleigh waves R_3/R_4 on a semilog scale. Directivity for exponentially decaying source as well as bilateral fault are also shown. Numerals near extremes indicate order of interference.

synthesis of the source time function from the initial phases and the corrected amplitude spectrum is possible. With the exception of unlikely favorable conditions, most records of major earthquakes do not show readable traces of R_1, which is the important phase for the study of the source mechanism. The recorded wave train of R_3 in the Mongolian earthquake did not contain the very high and the very low frequencies because of severe scattering and attenuation near the source, and the instrumental response. Time functions synthesized without them would correspond to a source function filtered with a band-pass filter. Depending on the band width, this function would be oscillatory, and it will not necessarily give rise to a time function similar to the original.

Error analysis. It is not feasible to present an exact quantitative figure for the upper limit of the errors in the spectra. However, even a semiqualitative analysis will be helpful in judging the accuracy of the results. The errors are due to two main causes:

1. Noise present in the record. This will include all signals other than the desired Rayleigh wave train. It is obvious from Figures 2 and 4 that the records are not noise free. The 'visible' noise is concentrated mainly at the short periods. A coherence test indicated that the coherence between R_3 and R_5 was much better at periods longer than 125 sec than that for shorter periods. Filtering, however, eliminated the noise of 40 sec and less.

2. Errors introduced through the numerical analysis. These errors are less readily detectable. They could come from many sources and may accumulate. Most significant of these are (*a*) errors in digitization, (*b*) effect of the finite window, and (*c*) errors of the finite integration process and round-off error of the computer. Digitization error should be relatively small, but the other factors require more attention.

TABLE 3. Initial Phases of Some Elementary Point Sources

$$tg\ \delta_0 = -\frac{\int_0^\infty G(t)\ \sin\ \omega t\ dt}{\int_0^\infty G(t)\ \cos\ \omega t\ dt}$$

	Time Function		
	$G(t)$*	Character	$-\delta_0\ (\omega > 0)$
1.	$\delta(t)$	Delta function	Zero
2.	$H(t)$	Unit step-function	$\pi/2$
3.	$H(t) - H(t - a)$	Rectangular pulse	$\omega a/2$
4.	$H(t)t^p e^{-\beta t}$	Gamma-kernel	$(1 + P)\ \tan^{-1}\frac{\omega}{\beta}$
5.	$H(t)e^{-\beta t}\cos\ \alpha t$	Attenuated cosine-wave	$\tan^{-1}\left\{\frac{\omega}{\beta}\left[1 - \frac{2\alpha^2}{\alpha^2 + \beta^2 + \omega^2}\right]\right\}$
6.	$\{H(t) - H(t - L)\}\ \sin\ \omega_0 t$	Finite sine-wave of K periods $(L = KT_0)$	$\frac{1}{2}(\omega L - \pi)$
7.	$H(t)[1 - e^{-\beta t}]$	Unit 'build-up' function	$\pi - \tan^{-1}\frac{\beta}{\omega}$
8.	$H(t)t^{-p}$	Hyperpolic decay	$\frac{\pi}{2}(1 - P) = \text{constant}$

* $\alpha > 0, \beta > 0$.

The effect of the finite window could be serious if the pulse had sufficient power outside it. In our case the seismograph attenuated the long periods (i.e. at 400 sec the response is 200 times less than the peak value) and the filtering took care of the short periods. Hence the power outside the window should be a very small fraction of the total power. Generally, for a square window of length L and a true spectrum $g(\omega)$, the computed spectrum is given by the convolution integral

$$F(\omega) = \int_0^\infty g(\omega - x)\frac{\sin\ xL/2}{xL/2}\,dx \qquad (13)$$

The solution of this integral equation for $g(\omega)$, especially for spectra as complicated as those of R_3 and R_4, is a difficult undertaking, if possible at all. The effect of the signal power outside the window may result in oscillations in $F(\omega)$. Since we ruled out this possibility, the oscillations in spectra, and hence the directivity, are most likely due to a constant-frequency undamped noise and partly to the interference of odd- and even-order Rayleigh waves which is constructive at discrete frequencies corresponding to those of free oscillations of the earth. However, the free oscillations alone can account for only about 1 per cent or less of the power of the oscillation of the spectra. The error of the numerical integration is bounded and its maximum value can be evaluated. Normally these errors are less than 10^{-3} times the value of average amplitudes, and they are completely negligible everywhere except maybe at the zeros of the spectra. Similarly, the round-off error of the computer is of no significance at frequencies other than the minimal points. The cumulative effect of all the errors is observable at the minima of spectra, and the phases are ill-behaved at these points. As the order of the Rayleigh wave passage increases, the signal-to-noise ratio decreases, and the errors increase, decreasing the reliability from R_3 to R_6.

The effect of the error on amplitudes is of no great significance in our case. However, in dealing with the phases we need much greater accuracy, and this limits the frequency range where the phases are reliable. Fortunately, the phase velocity is a slowly varying function of phases, and any error made in the phase results in a small error in phase velocity. For example, at the period of 100 seconds, if the phase has an error of $\pm\pi$, the error in phase velocity will be ± 0.02 km/sec, or less than ± 0.5 per cent.

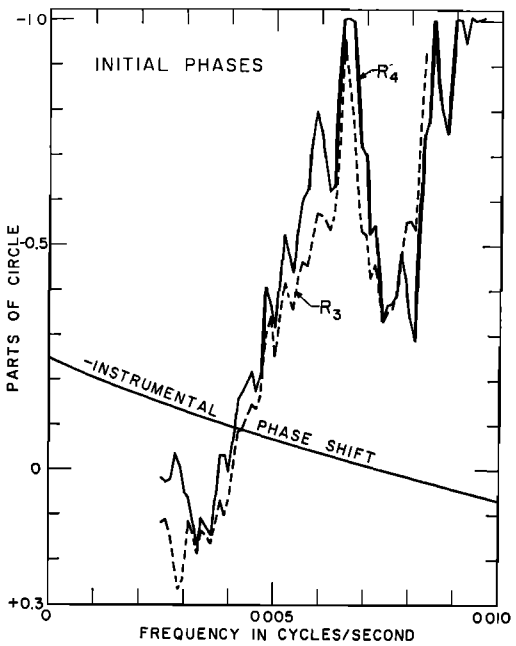

Fig. 12. Initial phases of R_3 and R_4. Phases have not been corrected for the instrumental phase shift.

Therefore the effect of the numerical errors on the phase velocities is insignificant.

Auxiliary Data

Geologic studies of the fault area. Two expeditions, one Mongolian and another from the East Siberian branch of the Academy of Sciences of USSR, were sent to the epicentral area. A detailed study was reported by N. A. Florensov, who headed the Soviet expedition that reached the area on January 2, 1958. The following quotations from this report give the information pertinent to our present study.

From the initial epicenter the ruptures extended only to the east, along the foothills of the Gurban-Bogdo chain for 270 km. . . . The flanks of the Bogdo fault were displaced vertically from 1.5–2 m to 10–12 m relative to one another, the southern, uphill side being upthrown and the northern, downhill side being downthrown. Moreover, at a series of points, the southern upthrown flank was displaced horizontally to the east, and the northern downthrown flank to the west by 3–3.5 m. Fractures of smaller extent, but still several tenths of kilometers in length, also enveloped the mountain chain on the south.

Another system of fractures leads along the low mountain boundary between the Yihe-Bogdo and the Baga-Bogdo massifs in an almost meridional direction and unites on the north with the major Bogdo fault. The frontal, eastern fracture 25–30 km in length is a crack whose edges are compressed, the western flank being lifted above the eastern by 2–3 to 6–10 meters. This is a result of a transverse thrust, occurring in the direction of the general movement from west to east.

Aftershocks and initial P motions. The distribution of the aftershocks, as reported by the Soviets, during the first year after the main shock is illustrated in Figure 10. About 200 large aftershocks were reported, 30 of which had magnitudes between 4 and 6½. The map indicates an aftershock area about 500 km long and 200 km wide. The aftershock distribution agrees with the fault trace and checks the fault length of 560 km obtained through our analysis.

A chart on initial P motions based on reports from 40 stations around the world is shown in Figure 13. It seems that the Byerly-Hodgson method is not of help to us in the determination of the dip angle: in spite of the fact that the direction of faulting is known, there is no apparent way of passing the circles without violating the orthogonality criteria. Thus this chart serves mainly to check the geological field reports while reflecting once more the great complexity of the source.

Air waves. Air waves which originated during the Mongolian earthquake were recorded on sensitive microbarographs at a distance of 2440 km northeast of the epicenter [*Passechnik*, 1959]. Lacking a readable copy of the original microbarogram, we shall quote the findings of I. P. Passechnik: 'The arrival of the air wave is obviously odd, and the oscillations have quasi-sinusoidal character. The lack of clear-cut air wave arrivals on the record, and of a sharply expressed anomalous dispersion, characteristic for powerful surface shots, and the relatively long duration of the oscillation (about 10 minutes) may be an indication that the source of the air wave did not have the characteristic of a well defined pulse.' One should be able at this point to estimate the fault length from the duration of the record. The contribution of the finite fault to the length of the air signal is given approximately by

$$(\Delta t)_1 = \left| \frac{\Delta_0}{V_a} - \frac{1}{V_a} \cdot \sqrt{\Delta_0^2 + b^2 - 2b\,\Delta_0 \cos\theta_0} - \frac{b}{V_f} \right|$$

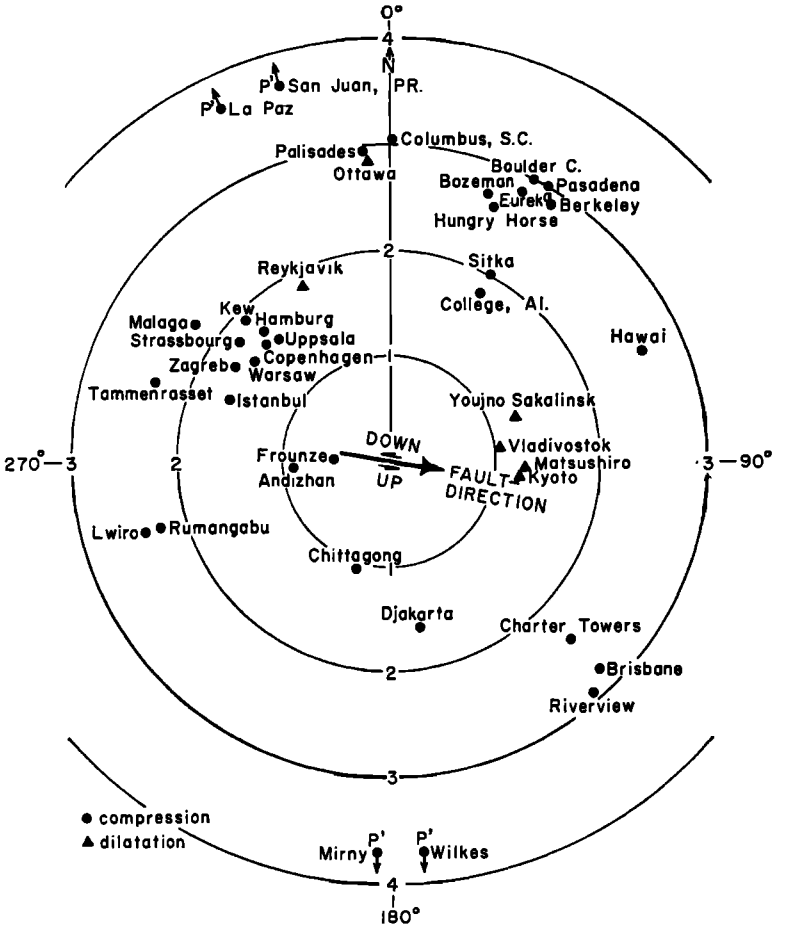

Fig. 13. A stereographic projection chart showing initial P motion as recorded on the seismograms of 40 stations around the earth.

where $\Delta_0 = 2440$ km is the distance of the recording station from the initial epicenter, $V_a = 0.320$ km/sec is the air-wave speed, b is the fault length, $V = 3.5$ km/sec is the rupture speed, and $\theta_0 = 55°$ is the angle at the station measured from the fault line. With these values we find $(\Delta t)_1 = 11.4$ min. Allowing for dispersion which cannot be significant for air waves of period 4 to 8 sec, traveling in a low-velocity layer, we come close to the observed value of 10 min. Obviously this observation is not accurate enough to determine the speed of rupture.

Depth estimation. The violent local destructions at the epicenter, the weak body waves with unclear onsets, and the high intensity of surface waves, recorded by most seismological stations around the globe, indicate a shallow focus. This is also confirmed from strain-release considerations [*Benioff*, 1951; *Båth and Benioff*, 1958]. Considering an aftershock area of 200 × 500 km (Fig. 10), we find an average depth of 50 km for an energy release of 10^{24} ergs.

Conclusion

Combining the various results obtained from our analysis together with the auxiliary data, we obtain a certain picture. Although its details are self-consistent we strongly feel that this picture is incomplete. This is mainly because our data did not include the information which was essential for the complete reconstruction of the source time function. This function is undoubtedly one of the important keys to the understanding of the processes which take place

at the epicenter at the time of origin. Valuable information stored in R_1, R_2, and P waves could not be recovered owing to instrumental shortcomings. It is highly desirable in future work to do the analysis simultaneously for records of a number of widely separated stations.

Appendix

Theorem. The only class of real one-sided time functions which possesses a constant phase spectrum are those of the form

$$H(t)t^{-\beta} \qquad (\beta,\ t \text{ real})$$

Proof. Let the spectrum of $G(t) = H(t)g(t)$ be given by $S(\omega)e^{-i\delta(\omega)} = exp\ -[A(\omega) + iB(\omega)]$. We now invoke the 'phase-integral theorem' [*Richards*, 1959]:

$$A(\omega) - A(0) = -\frac{\omega}{\pi}\int_0^\infty \frac{d}{dx}\left(\frac{B}{x}\right) \ln\left|\frac{x+\omega}{x-\omega}\right| dx \qquad (1)$$

Substituting the condition $\delta = \delta_0 =$ constant and evaluating the divergent integral in (1), we find

$$\int_0^\infty \ln\left|\frac{x+\omega}{x-\omega}\right| \frac{dx}{x^2} = \frac{2}{\omega}\ln\omega - \frac{2}{\omega}\lim_{x\to\infty}\ln x \qquad (2)$$

Equating the divergent part of (2) to $A(0)$ we have

$$S(\omega) = \omega^{-2\delta_0/\pi} \qquad (3)$$

For a delta function $\delta_0 = 0$; hence $S(\omega) = 1$. For a unit step function $\delta_0 = \pi/2$; therefore $S(\omega) = 1/\omega$ as it should. To obtain the time function from (3) we put $S(\omega) = S(-\omega)$ and $\delta = \delta_0 \operatorname{sgn}\omega$.

Thus

$$g(t) = \frac{2}{\pi}\int_0^\infty \frac{\cos(\omega t - \delta_0)}{\omega^\gamma}\, d\omega = \frac{2}{\pi}\Gamma(\beta)t^{-\beta}\sin 2\delta_0 \qquad (4)$$

$$\gamma = \frac{2\delta_0}{\pi};\quad \beta = 1-\gamma;\quad \delta_0 = \frac{\pi}{2}(1-\beta) \qquad (5)$$

The real values of β and γ are unrestricted. Integer values of β correspond to the delta function, its derivatives, and integrals.

Acknowledgments. This research was supported by Contract Af-49 (638) 910 of the Air Force Office of Scientific Research as part of the Advanced Research Projects Agency project VELA. We wish to thank Dr. Stewart W. Smith and Mr. Shelton S. Alexander for helping us with the digital analysis. Acknowledgment is also due Gilbert Dewart for translation of a foreign text, and Laszlo Lenches who drew the figures. Group velocities in Figure 9 were computed by Eli Arieh and Don L. Anderson.

References

Båth, M., and H. Benioff, The aftershock sequence of the Kamchatka earthquake of November 4, 1952, *Bull. Seism. Soc. Am., 48,* 1–15, 1958.

Benioff, H., Earthquakes and rock creep, 1, *Bull. Seism. Soc. Am., 41,* 31–62, 1951.

Ben-Menahem, A., Radiation of seismic surface waves from finite moving sources, *Bull. Seism. Soc. Am., 51,* 401–435, 1961.

Ben-Menahem, A., Radiation of seismic body waves from a finite moving source in the earth, *J. Geophys. Research, 67,* 369–374, 1962.

Brune, J. N., Radiation pattern of Rayleigh waves from the southeast Alaska earthquake of July 10, 1958, *Symposium on Earthquake Mechanism, Publs. Dominion Observatory, Ottawa, 24,* 10, 1961.

Brune, J. N., H. Benioff, and M. Ewing, Long-period surface waves from the Chilean earthquake of May 22, 1960, recorded on linear strain seismographs, *J. Geophys. Research, 66,* 2895–2910, 1961.

Brune, J. N., J. E. Nafe, and L. E. Alsop, The polar phase shift of surface waves on a sphere, *Bull. Seism. Soc. Am., 51,* 247–257, 1961.

Florensov, N. A., Catastrophic earthquake in the Gobi Altai, *Priroda, 7,* 73–77 (Publication of the Academy of Science USSR) 1958.

Gilman, R., Report on some experimental long-period seismographs, *Bull. Seism. Soc. Am., 60,* 553–559, 1960.

Passechnik, I. P., Air waves occurring during the Gobi-Altai earthquake of December 4, 1957, *Izvest. Akad. Nauk SSSR, Ser. Geofiz.,* 1687–1689, 1959.

Press, F., A. Ben-Menahem, and M. Nafi Toksöz, Experimental determination of earthquake fault length and rupture velocity, *J. Geophys. Research, 66,* 3471–3485, 1961.

Press, F., Maurice Ewing, and Francis Lehner, A long-period seismograph system, *Trans. Am. Geophys. Union, 39,* 106–108, 1958.

Richards, P. I., *Manual of Mathematical Physics,* Pergamon Press, New York, 1959.

Tranter, C. J., *Integral Transforms in Mathematical Physics,* Methuen and Co. Ltd., London, 1956.

(Manuscript received December 22, 1961; revised February 7, 1962.)